Short-Term Regional Temperature and Salinity Prediction Based on Deep Learning Long Short-Term Memory

Kara Lin

University of Washington

School of Oceanography, Box 357940 Seattle WA 98195-7940

lincan@uw.edu

03/07/2025

Abstract

The El Niño-Southern Oscillation (ENSO) is the most significant year-to-year climate variation, affecting weather and climate systems worldwide. However, current prediction models, both dynamic and statistical, struggle with accuracy due to the complex mechanism of ENSO. This study introduces a regional temperature and salinity prediction method using a Long Short-Term Memory (LSTM) deep learning model, which is well-suited for identifying long-term patterns in sequential data. The model is applied to three specific regions using in-situ data from Argo floats: the central-eastern Pacific, the central tropical Pacific Niño 3.4 region, and the Western Pacific Warm Pool (WPWP). These regions are chosen because they play key roles in ENSO dynamics. Results show that the LSTM model performs best in the WPWP, where the average mean squared error (MSE) is low (0.03), indicating high accuracy and stability. This is likely due to lower noise in the original data. In contrast, the model performs poorly in the central-eastern Pacific, where the average MSE is much higher (7.03), suggesting instability due to high noise in original data. These findings highlight the potential of deep learning for regional climate predictions and suggest that LSTM models could improve local weather forecasting and fisheries management.

Plain Language Summary

The current studies focus on predicting the El Niño-Southern Oscillation (ENSO) in the Central Equatorial Pacific (Niño 3.4 region) using various statistical and machine learning (ML) models. El Niño-Southern Oscillation (ENSO) is a major climate pattern that affects weather worldwide, influencing everything from storms to droughts. Scientists use different models to predict ENSO, but these models often struggle because ENSO is complex and behaves differently across regions. This study looks at how well a deep learning model, called Long Short-Term Memory (LSTM), can predict ocean temperature and salt levels in three key areas: the Central-Eastern Pacific, the Niño 3.4 region, and the Western Pacific Warm Pool (WPWP). The LSTM model, an advanced recurrent neural network capable of capturing and learning long-term repeating signals in time-series data, is well-suited for capturing ENSO's long-term signals. Since ENSO characteristics differ across these three regions, the model's predictive performance is expected to vary accordingly. Results show that the LSTM model performs best in the WPWP, where the error between the actual and prediction (mean squared error: MSE) is low (0.03), indicating high accuracy and stability in the original real data. In contrast, the model performs poorly in the central-eastern Pacific, where the average MSE is much higher (7.03), suggesting instability due to high noise in original data. By comparing the LSTM model's accuracy across these regions, this study will provide insights into its strengths and limitations in forecasting ENSO at different stages. A better understanding of these regional differences will help improve prediction models, ultimately helping local governments in disaster precautions and supporting fisheries management.

1 Introduction

The El Niño-Southern Oscillation (ENSO) stands as one of the most influential climate phenomena globally, exerting profound impacts on weather patterns, oceanic conditions, and ecosystems worldwide (Rasmusson, 1985). Its effects are far-reaching, extending from the tropics to the mid-latitudes and beyond. El Niño and La Niña are the two primary phases of ENSO. Both are the result of ocean-atmosphere interactions (Dawson & O'Hare, 2000). During El Niño events, the eastern and central tropical Pacific waters become warmer than average. In contrast, during La Niña events, water will be cooler than average (Ibebuchi & Richman, 2024).

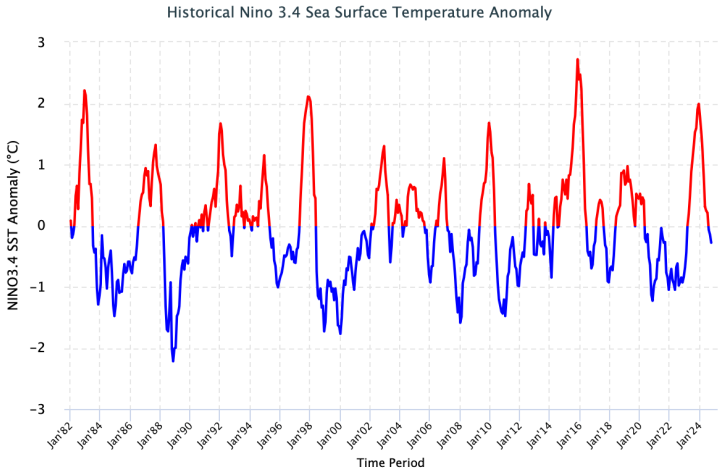

Figure 1. Niño 3.4 Sea Surface Temperature Anomaly

The Niño 3.4 anomaly index is widely used as an indicator and predictor of ENSO. It represents the average sea surface temperature (SST) anomalies in the central equatorial Pacific (Figure 1). Specifically, it uses a 5-month running mean in the region between 5°N–5°S and 170°W–120°W, where the ocean and atmosphere show strong sensitivity to each other's variations. El Niño and La Niña events are defined by anomalies of ±0.4°C (Schneider et al., 2013). This index provides valuable insights into how ENSO impacts those regions.

The Niño3.4 region and the central-eastern Pacific exhibit significant variability in temperature and salinity due to the influence of ENSO events (Trenberth, 1997). During an El Niño event, weakened trade winds allow warm surface waters to expand eastward from the central Pacific, increasing sea surface temperatures (SSTs) in the Niño3.4

region and the central-eastern Pacific. This shift suppresses the usual upwelling of cold, nutrient-rich water, leading to higher temperatures and reduced salinity due to increased precipitation and reduced mixing with deeper saline waters. Conversely, during La Niña, stronger trade winds enhance the upwelling of cold, nutrient-rich water along the eastern Pacific, lowering SSTs and increasing salinity as evaporation intensifies and precipitation shifts westward. These oceanic and atmospheric changes play a crucial role in global climate variability, impacting regional weather patterns, marine ecosystems, and fisheries along the South American coast.

The Western Pacific Warm Pool (WPWP) is a region of the Pacific Ocean with some of the warmest SSTs in the world, extending from the eastern Indian Ocean to the central Pacific (Chen et al., 2021). During an El Niño event, the trade winds weaken, allowing the warm waters of the WPWP to shift eastward toward the central and eastern Pacific. This shift disrupts the normal atmospheric and oceanic conditions, suppresses the upwelling of cold water in the east. Conversely, during La Niña, the WPWP's warm waters are more confined to the western Pacific, intensifying the temperature gradient and trade winds, which enhances upwelling in the eastern Pacific and reinforces the normal climate pattern. Therefore, the WPWP's behavior is the opposite of the Niño3.4 region and the central-eastern Pacific.

Temperature and salinity prediction are often approached as time series forecasting problems, though they are also commonly studied using 4D physical models. Deep learning has become a popular approach for handling nonlinear time series predictions (Ismail Fawaz et al., 2019). However, predicting ocean temperature and salinity presents challenges due to the complex data structures and varying features over time (Wu et al., 2022). To address these challenges, Long Short-Term Memory (LSTM) networks have proven particularly effective. Long Short-Term Memory networks (LSTMs) are a specialized type of recurrent neural network (RNN) designed to effectively model and predict time series data by capturing long-range dependencies. Traditional RNNs process data sequentially, where information from previous time steps is passed along to later ones. However, they face a significant limitation known as the vanishing gradient problem (Mu et al., 2020). This issue occurs during training when gradients used to update the model's weights become so small that the network struggles to learn relationships between distant time steps, resulting in poor performance for long-term dependencies. LSTMs address this limitation with a unique architecture that includes three main com-

ponents: gates, a cell state, and hidden states. The input gate determines what new information should be added to the memory. The forget gate decides what information from the past should be discarded. The output gate controls the flow of information from the memory to the output at the current step. These gates allow the network to selectively add, retain, or remove information at each time step. These mechanisms work together to maintain a stable and persistent cell state, which acts as the network's memory, enabling it to retain critical information over extended sequences. As a result, LSTMs can capture long-term patterns and trends in sequential data, making them highly effective for tasks like weather forecasting, natural language processing, stock market analysis, and ENSO predictions (Ibebuchi & Richman, 2024). By overcoming the limitations of traditional RNNs, LSTMs have become a cornerstone in time series analysis and forecasting.

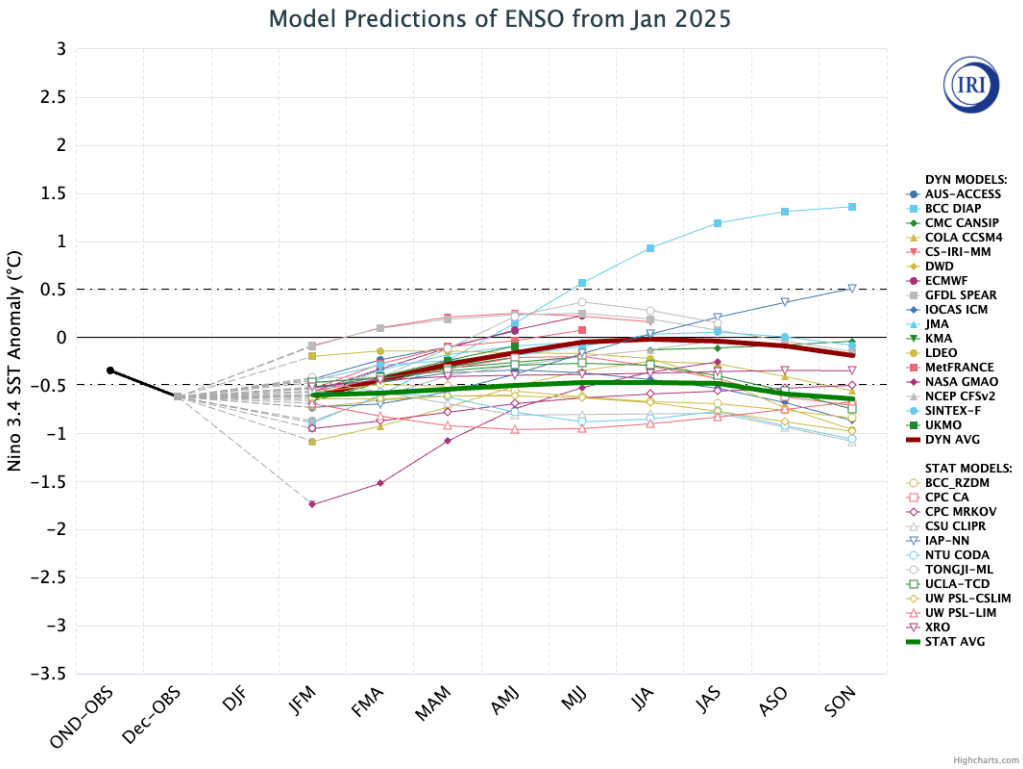

Figure 2. Forecasts of the Nino3.4 SST anomaly from dynamical and statistical models that are run during the first half of the month. Figure provided by the International Research Institute (IRI) for Climate and Society updated January 2025.

LSTM networks are particularly well-suited for ENSO prediction due to their ability to capture long-term dependencies and patterns in sequential data (Ibebuchi & Richman, 2024). LSTM model is not used by IRI and their models have a wide range of variation (Figure 2). Unlike traditional models, which often struggle to effectively incorporate information from the past, LSTMs are designed with memory cells that selectively retain or discard information over time. This capability is crucial for ENSO prediction, as ENSO events develop gradually and are influenced by processes that can span months to years. LSTM models can capture these slow-evolving signals, tracking the complex interactions within the ocean-atmosphere system that are essential for forecasting El Niño or La Niña events. Furthermore, LSTMs handle non-linear relationships, enabling them to identify subtle patterns in climate data that may be overlooked by linear or shallow models. By leveraging their memory and non-linearity capabilities, LSTMs have the potential to provide more accurate and reliable ENSO predictions, surpassing traditional statistical models and other machine learning methods that cannot fully exploit temporal dependencies in the data.

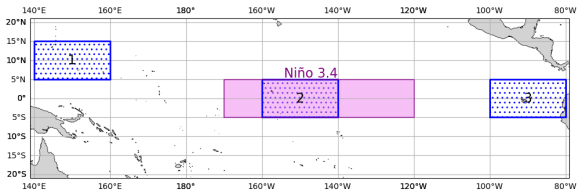

Figure 3. Box coordinates.

In this study, an LSTM model is developed to predict temperature and salinity in three regions, extending beyond the traditional Niño 3.4 index boundaries. The Niño 3.4 index typically relies on data from a narrow equatorial band (5°S to 5°N) (Figure 3), but this model expands the input data range to 5°S to 15°N, encompassing a broader tropical region. In-situ data were collected at 15°N by three Argo floats, which are autonomous, free-drifting instruments that monitor temperature, salinity, and, in some cases, additional parameters such as dissolved oxygen at various depths. The influence of these expanded northern latitudes on the model's predictions is intriguing to explore. Since the Niño 3.4 region (5°S to 5°N) has a strong influence on ENSO dynamics, one might expect that the model's accuracy could primarily depend on data from this equatorial zone. The study will help determine the model's performance on predicting temperature and salinity in three key regions of the Pacific: WPWP (10°N to 15°N, 140°E to 160°E, Box 1), the Niño3.4 region (5°S to 5°N, 140°W to 160°W, Box 2), and the central-

eastern Pacific (5°S to 5°N, 80°W to 100°W, Box 3). Predictions were made at depths of 10 m, 20 m, and 100 m to capture vertical variations in ocean properties. By analyzing how the predictions differ across regions and depths, this study aims to provide insights into the model's performance and the underlying oceanographic processes influencing temperature and salinity variability. This approach could reveal whether the predictive power of the LSTM model is more sensitive to the dominant ENSO signals in the equatorial region or if the additional data from northern latitudes contributes valuable insights that refine its forecasts.

2 Method

2.1 Data Acquisition and Pre-Processing

Three in-situ Argo floats were deployed (Figure 4) during Dec 29, 2024 - Jan 10, 2025 *R/V Thomas G. Thompson* senior thesis cruise. They record temperature and salinity down to 1000 m and send back the data at a 10-day frequency. These 3 Argo floats will not be recycled but permanently left in the ocean to continue recording data in the next 10 years.

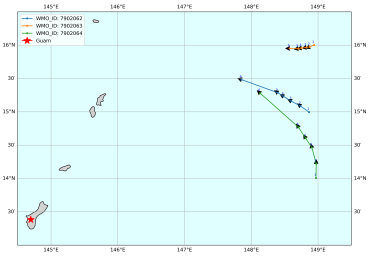

Figure 4. In-situ Argo floats paths.

Argo DOI files since July 1, 2014 till January 9, 2025 in the entire tropical Pacific region were obtained from Argo GDAC (Argo, 2025). Temperature and salinity data in the in-situ region (upper left: 15°N, 140°E; lower right: 5°S, 80°W) were obtained from Argo DOI files. The raw NetCDF data was cleaned, and temperature, salinity, coordinates, and time were written into a new CSV file. The Roemmich-Gilson (RG) 14-year consecutive climatology mean (Roemmich & Gilson, 2009) of the temperature and salinity is used as the gridded averaged climatology for the calculation. The data is organized into a 1° x 1° grid for longitude and latitude. When multiple data points (Argo profiles) fall within the same grid cell, their average is used for further analysis and modeling, resulting in an average of 1850 grid points for each 126 monthly time steps. Data was then normalized by calculating the anomaly and dividing by the standard deviation (SD). Then, for each region (box), the average of each parameter at each depth and each time point

are taken as the final input dataset. This normalization is shown in Equation 1:

$$C_{(x_i,y_i),t,z} = RC_{(x_i,y_i)} - MC_{(x_i,y_i)}$$
$$C(t,z) = \frac{1}{n}\sum_{i}^{n} C_{(x_i,y_i),t,z} \tag{1}$$

where (x_i, y_i) is the geostrophic data point, x stands for longitude and y stands for latitude. C is the parameter of interest, either temperature or salinity. t is the time series. z is the depth. RC is actual data from Argo floats, MC is the RG gridded consecutive climatology, $SDRC$ is the standard deviation of the real data.

To just observe the variability in each parameter beyond the predictable annual fluctuations, the seasonal cycle is removed from the actual training dataset. This is necessary because temperature and salinity exhibit strong seasonal patterns, and a good model should focus on predicting deviations from this repeating cycle rather than the cycle itself. The seasonal cycle is removed by fitting a harmonic function to the data using a least-squares approach and then subtracting the fitted function. The harmonic function used to model the seasonal cycle is given by Equation 2. Although the input dataset is already in anomaly form (actual - mean), additional seasonal cycle removal helps eliminate residual periodicity, ensuring that the model captures non-seasonal variability more effectively (Nelson et al., 1999).

$$S(t,z) = a\sin\frac{2\pi t}{365} + b\cos\frac{2\pi t}{365} + c\sin\frac{4\pi t}{180} + d\cos\frac{4\pi t}{180} + e \tag{2}$$
$$C(t,z)_{deseasonalized} = C(t,z) - S(t,z) \tag{3}$$

where $S(t,z)$ is the harmonic equation to model the seasonal cycle. a, b, c, d, e are fitted parameters. a, b, c, d: amplitudes of the sine and cosine components. a, b will remove the annual cycle, and c, d will remove semi-annual cycle. c: mean offset. t: fractional time, the day of the year.

An running mean filter (Equation 4) is applied to smooth the data by averaging over a sliding window (5 days), effectively reducing short-term noise.

$$C(i)_{smoothed} = \frac{1}{5}\sum_{i=-2}^{n=2} C(t+i,z) \tag{4}$$

2.2 LSTM Prediction Model

The predictive deep learning model was defined using a dataset of both the input predictors (normalized time series temperature and salinity data) and the predict and

output (Niño 3.4 index) (Ibebuchi & Richman, 2024). For training and testing, the dataset was divided into an 80% training subset (July 1, 2014 to Jan 25, 2023) and a test subset from Jan 26, 2023 to Jan 9, 2025. This partitioning ensures that both subsets contain complete ENSO events. Although the time span can be extended back to 2002, a smaller, manageable dataset was chosen initially for ease of analysis.

The LSTM model was implemented with layers designed to capture long-term dependencies. A combination of hyper-parameters, such as the number of neurons in each layer, learning rate, and dropout rate, was optimized to prevent over-fitting and improve performance. The model was trained using back-propagation through time, employing an Adam optimizer to minimize the mean squared error (MSE) loss function. The validation dataset was used to monitor training progress, with early stopping implemented to halt training when validation loss ceased improving.

Figure 5 shows the flow chart in applying the LSTM model. LSTM neurons are a type of recurrent neural network structure designed to capture long-term dependencies in sequential data, making them well-suited for time series forecasting. In our model, the input layer consists of a sequence of past observations with a single predictor variable. The LSTM layer contains 50 neurons, a choice determined through experimental evaluation to balance model complexity and predictive accuracy. The output layer is a single dense neuron that produces the final prediction. This architecture allows the model to effectively learn temporal patterns while avoiding overfitting.

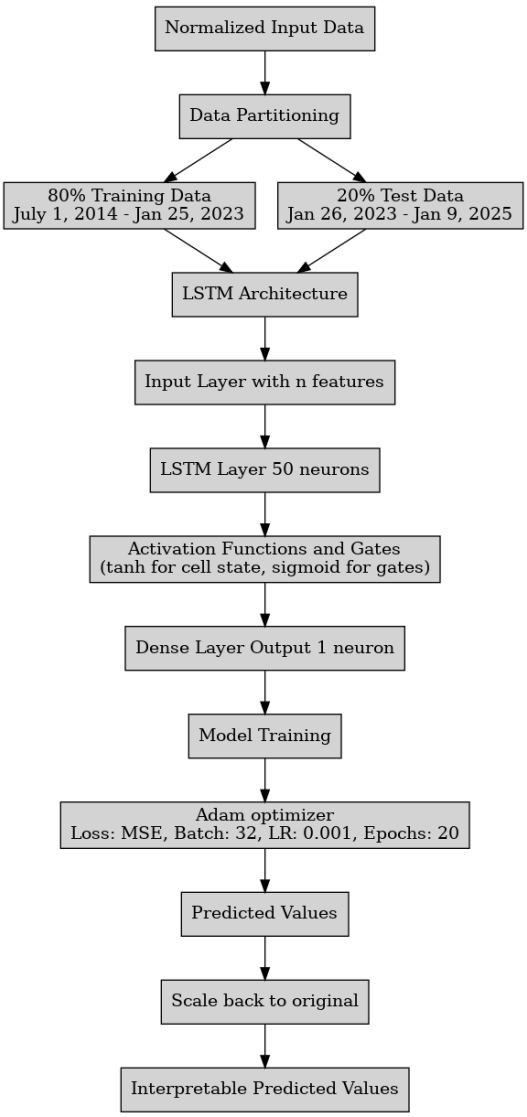

Figure 5. Flow chart in applying the LSTM for temperature and salinity predictions (Ibebuchi & Richman, 2024).

2.3 Experimental Results and Visualization

To evaluate how well the LSTM model performs in each region, the average performance metrics are preformed, such as accuracy: mean squared error (MSE, Equation 5), root mean squared error (RMSE, Equation 1), mean average error (MAE, Equation 7). MSE measures the overall prediction error. RMSE measures the standard deviation of prediction errors, providing a measure of the magnitude of the error. MAE measures the average magnitude of errors in a set of predictions, without considering their direction. The lower the error metrics indicates better model performance. And the Corre-

lation coefficient measures the strength and direction of the linear relationship between observed values (C_i) and predicted values ($\hat{C}_i$). Finally, or error distributions (for regression tasks) were analyzed to visually compare the performance and stability of the model with each dataset, giving a comprehensive view of which input data produces a more accurate LSTM model.

$$\text{MSE} = \frac{1}{N}\sum_{i=1}^{N}(C_i - \hat{C}_i)^2 \tag{5}$$

$$\text{RMSE} = \sqrt{\frac{1}{N}\sum_{i=1}^{N}(C_i - \hat{C}_i)^2} \tag{6}$$

$$\text{MAE} = \frac{1}{N}\sum_{i=1}^{N}|C_i - \hat{C}_i| \tag{7}$$

$$r = \frac{\sum_{i=1}^{N}(C_i - \bar{C})(\hat{C}i - \bar{\hat{C}})}{\sqrt{\sum i = 1^N (C_i - \bar{C})^2}\sqrt{\sum_{i=1}^{N}(\hat{C}_i - \bar{\hat{C}})^2}} \tag{8}$$

3 Results

Figure 6 shows the temperature anomaly at 10 m depth in the WPWP region (Box 1). The temperature and salinity anomalies for the other regions (Boxes 1, 2, and 3) are not shown, as they have similar trends. There is a distinct seasonal cycle, with temperature anomalies peaking in the summer months and reaching their lowest points in winter. In winter 2015 - 2016, the temperature in the WPWP is lower than in other years' winters, shown by greater than -1°C anomaly, which is a signal for El Niño. During El Niño years, the water is colder than usual in the Western Pacific. In Figure 1, 2016 is a high temperature (El Niño) year in the Central and Eastern Pacific. Both result agrees.

The smoothed temperature anomaly (blue dashed line) exhibits fewer extreme fluctuations compared to the actual historical data (light blue solid line). The test prediction (red dashed line) aligns up with the historical data every well that it almost overlaps all the peaks. The deseasonalized anomaly has a clear offset than the actual historical anomaly, no more clear seasonal signals, demonstrating that removing the seasonal cycle does alter the overall trend. The statistical error metrics, including MSE, RMSE, and MAE, are consistently lower for the smoothed data compared to the unsmoothed data. For instance, in Box 2 at 10 m depth, the MSE for the unsmoothed data is 0.18, whereas the MSE for the smoothed data is significantly lower at 0.05 (Table 1). A sim-

ilar trend is observed in RMSE and MAE values. The statistical error metrics for temperature anomaly are lower in Box 1 and Box 2 compared to Box 3 in the shallow water depth (10 m, 20 m). For Box 1 and Box 2, the error metrics are lower in the shallow water than deeper water. However, for Box 3, the error metrics is lower in the deep water than the shallow water. The correlation coefficient for the temperature smoothed data is high (greater than 0.9) at all depths across all three regions. The salinity statistical results have really different trend than temperature. The error metrics is only low at Box 1 in all depths but very high (over 1) for all depth in Box 2 and 3. The unsmoothed correlation coefficient is relative high in Box 1 (over 0.6) but low in Box 2 and Box 3 (less than 0.5). The smoothing filter also does decrease error metrics in all three regions for salinity dramatically and increase the correlation coefficient.

Table 1. Temperature($^{\circ}C$) prediction performance for each three box at each depth, where the train/test ration is 0.8.

	Box 1			**Box 2**			**Box 3**		
	10	**20**	**100**	**10**	**20**	**100**	**10**	**20**	**100**
MSE	0.04	0.05	0.94	0.18	0.16	0.55	0.84	1.17	0.34
MSE Smoothed	0.01	0.06	0.16	0.05	0.03	0.21	0.17	0.26	0.08
MSE Deseasonalized	0.04	0.06	0.97	0.17	0.20	1.16	0.90	1.21	0.43
RMSE	0.20	0.23	0.97	0.42	0.40	0.738	0.91	1.08	0.63
RMSE Smoothed	0.10	0.12	0.39	0.23	0.18	0.47	0.41	0.51	0.29
RMSE Deseasonalized	0.22	0.25	0.99	0.41	0.42	1.08	0.95	1.10	0.66
MAE	0.16	0.17	0.75	0.32	0.30	0.55	0.70	0.85	0.47
MAE Smoothed	0.08	0.10	0.30	0.18	0.13	0.35	0.30	0.41	0.22
MAE Deseasonalized	0.16	0.19	0.76	0.31	0.34	0.83	0.73	0.85	0.50
Corr	0.94	0.92	0.38	0.93	0.93	0.70	0.80	0.74	0.74
Corr Smoothed	0.98	0.97	0.87	0.98	0.99	0.92	0.95	0.93	0.93
Corr Deseasonalized	0.72	0.64	0.51	0.91	0.91	0.67	0.74	0.71	0.67

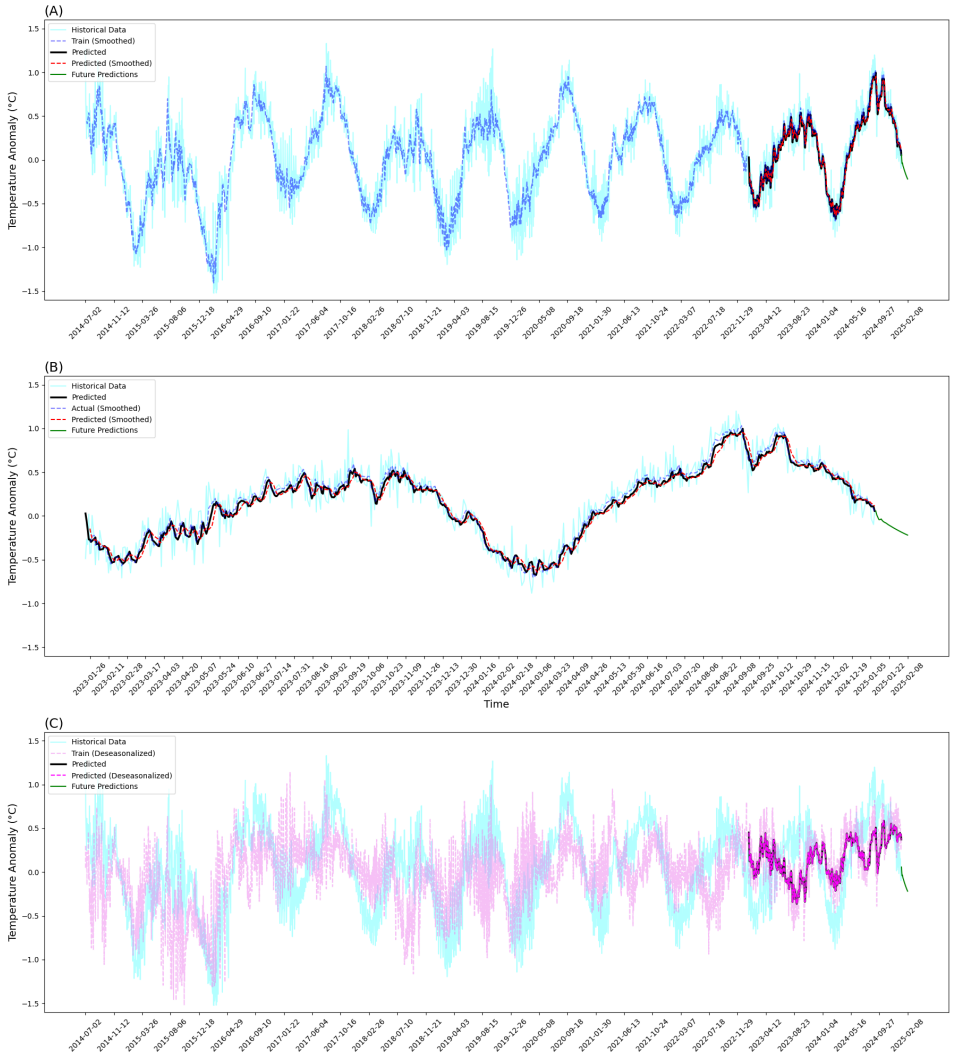

Figure 6. Temperature anomaly in the WPWP region (Box 1) at a depth of 10 m. The top panel (A) displays both the training and test datasets of historical data, historical smoothed data, test predictions, and a 30-day future prediction. The middle panel (B) shows only the test dataset, including historical data, test predictions, and a 30-day future prediction. The bottom panel (C) displays both the training and test datasets of historical data, seasonal removed historical data, test predictions, and a 30-day future prediction. The color legend is the same for all three panels. Light cyan solid line: real historical data. Light blue dashed line: smoothed historical data. Light purple dashed line: seasonal removed historical data. Black solid line: prediction in the test dataset. Pink dashed line: seasonal removed prediction in the test dataset. Green solid line: 30-day future prediction.

Table 2. Salinity (psu) prediction performance for each three box at each depth, where the train/test ration is 0.8.

	Box 1			**Box 2**			**Box 3**		
	10	**20**	**100**	**10**	**20**	**100**	**10**	**20**	**100**
MSE	0.02	0.03	0.02	1.03	1.06	1.19	7.36	7.45	7.09
MSE Smoothed	0.003	0.005	0.04	0.10	0.10	0.11	1.06	1.05	0.99
MSE Deseasonalized	0.02	0.02	0.02	1.08	1.01	1.19	8.31	8.33	7.92
RMSE	0.14	0.16	0.14	1.01	1.02	1.09	2.71	2.72	2.66
RMSE Smoothed	0.06	0.07	0.07	0.32	0.32	0.22	1.03	1.02	1.00
RMSE Deseasonalized	0.13	0.15	0.13	1.05	1.05	1.09	2.88	2.90	2.82
MAE	0.106	0.127	0.10	0.33	0.34	0.34	0.92	0.88	0.70
MAE Smoothed	0.05	0.06	0.05	0.14	0.15	0.13	0.43	0.42	0.32
MAE Deseasonalized	0.10	0.11	0.10	0.34	0.33	0.36	0.99	0.95	0.78
Corr	0.78	0.66	0.51	0.32	0.31	0.28	0.45	0.42	0.40
Corr Smoothed	0.92	0.89	0.83	0.81	0.82	0.82	0.84	0.82	0.83
Corr Deseasonalized	0.49	0.44	0.32	0.25	0.23	0.24	0.25	0.24	0.24

4 Discussion

4.1 Smoothing and Deseasonalization Effect on Model Performance

The performance of the LSTM model varies across different regions and depths. Surprisingly, the best performance is observed in the WPWP region (Box 1) a weak ENSO signal region, as indicated by lower statistical error metrics. The three evaluation metrics, MSE, RMSE, and MAE, collectively measure the magnitude and consistency of prediction errors. A lower value in these metrics suggests better model performance. Additionally, the correlation coefficient quantifies the strength of the linear relationship between observed and predicted values, where higher values indicate better predictive accuracy.

As shown in Tables 1 and 2, the model performs exceptionally well in the WPWP region, with low error metrics and high correlation coefficients for both temperature and salinity anomalies. In contrast, the Central and Eastern Pacific region exhibits higher prediction errors and weaker correlations, suggesting that the model struggles to capture variability in this area. The smoothing technique applied to the anomaly data reduces extreme fluctuations, leading to lower error metrics and improved correlation across

all depths (Alysha M. De Livera & Snyder, 2011). This suggests that removing high-frequency noise enhances the model's ability to detect meaningful patterns in temperature and salinity anomalies.

Based on simple visualization, the effectiveness of deseasonalization in this study seems to be well. However, the statistical results doesn't suggest that the deseasonalization improve the overall model prediction a lot which is contrary to Nelson et al. (1999)'s study. One possible reason would be that there is still some seasonal cycle that I haven't removed by 2, since this equation only remove the annual and semi-annual cycle. Another possible explanation is that the LSTM model is so good at capturing the annual variation, without the clear annual variation, the LSTM model won't perform as well as the deseasonalization.

4.2 Regional LSTM Model Performance on Temperature ans Salinity

The LSTM model exhibits different levels of predictive accuracy depending on the region and depth analyzed. The WPWP region shows strong predictive performance, likely due to the stable and persistent oceanographic conditions in this area. In contrast, the central-eastern Pacific presents greater challenges, as indicated by higher MSE, RMSE, and MAE values. One possible explanation for this discrepancy is the increased variability and complex ocean-atmosphere interactions in this region, particularly in relation to ENSO events.

Temperature predictions generally show higher accuracy than salinity predictions across all regions. This could be attributed to the fact that temperature data often exhibit stronger seasonal signals and are more directly influenced by large-scale oceanic processes, making them easier to model. Salinity, on the other hand, is affected by a range of complex factors, including precipitation, evaporation, and horizontal advection, which may introduce additional uncertainty into the model. The results suggest that while the LSTM model is effective in capturing temperature variability, further refinements may be necessary to improve salinity predictions.

5 Conclusions

This study developed and applied an LSTM model to predict temperature and salinity anomalies in three distinct oceanic regions, demonstrating varying levels of perfor-

mance across different locations and depths. The results indicate that the model performed best in the WPWP region, where statistical errors were lower, and correlation coefficients were consistently high. In contrast, predictions in the Central and Eastern Pacific exhibited higher errors and lower correlations, highlighting the challenges of forecasting in regions with complex variability. Additionally, smoothing the input data reduced extreme values and improved overall model accuracy, though its effectiveness varied by region. The findings emphasize the importance of regional differences in ocean dynamics when designing predictive models. The lower performance in the Central and Eastern Pacific suggests that standard deseasonalization techniques may not always enhance prediction accuracy, as they can potentially remove meaningful inter-annual variability, particularly in ENSO-dominated regions.

These results suggest that future work should explore alternative preprocessing techniques, such as adaptive filtering or region-specific data transformation methods, to better capture key oceanographic signals. Future studies can build upon this work by incorporating additional physical variables, such as wind stress or thermocline depth, which may improve predictive accuracy in regions with strong ocean-atmosphere interactions. Furthermore, testing hybrid models that integrate LSTM with traditional physical models could provide a more robust framework for forecasting oceanic anomalies. Ultimately, refining data preprocessing strategies and model architectures will be essential for improving long-term ocean prediction capabilities, which are critical for understanding and mitigating climate variability impacts.

Acknowledgments

I extend my deepest gratitude to the entire Ocean 445 teaching team, specifically to my supervisor, Professor Alison Gray, for her support. My appreciation also goes to my PI, Professor Steve Riser, for his insightful critiques throughout my research journey and for funding my research. His lab also provided the in-situ Argo floats. I would like to express my gratitude to the captain and crew of the *R/V Thomas G Thompson*, as well as Argo GDAC program.

References

Alysha M. De Livera, R. J. H., & Snyder, R. D. (2011). Forecasting time series with complex seasonal patterns using exponential smoothing. *Journal of the American Statistical Association*, *106*(496), 1513–1527. Retrieved from https://doi.org/10.1198/jasa.2011.tm09771 doi: 10.1198/jasa.2011.tm09771

Argo. (2025). Argo float data and metadata from global data assembly centre (argo gdac). *SEANOE*.

Chen, H., Shi, J., Jin, Y., Geng, T., Li, C., & Zhang, X. (2021). Warm and cold episodes in western pacific warm pool and their linkage with enso asymmetry and diversity. *Journal of Geophysical Research: Oceans*, *126*(12), e2021JC017287.

Dawson, A., & O'Hare, G. (2000). Ocean-atmosphere circulation and global climate: the el-niño-southern oscillation. *Geography: Journal of the Geographical Association*, *85*(3), 193.

Ibebuchi, C. C., & Richman, M. B. (2024). Deep learning with autoencoders and lstm for enso forecasting. *Climate Dynamics*, 1–15.

Ismail Fawaz, H., Forestier, G., Weber, J., Idoumghar, L., & Muller, P.-A. (2019). Deep learning for time series classification: a review. *Data mining and knowledge discovery*, *33*(4), 917–963.

Mu, B., Ma, S., Yuan, S., & Xu, H. (2020). Applying convolutional lstm network to predict el niño events: Transfer learning from the data of dynamical model and observation. In *2020 ieee 10th international conference on electronics information and emergency communication (iceiec)* (pp. 215–219).

Nelson, M., Hill, T., Remus, W., & O'Connor, M. (1999). Time series forecasting using neural networks: should the data be deseasonalized first? *Journal of Forecasting*, *18*(5), 359-367. Retrieved from https://onlinelibrary.wiley.com/doi/abs/10.1002/%28SICI%291099-131X%28199909%2918%3A5%3C359%3A%3AAID-FOR746%3E3.0.CO%3B2-P doi: https://doi.org/10.1002/(SICI)1099-131X(199909)18:5⟨359::AID-FOR746⟩3.0.CO;2-P

Rasmusson, E. M. (1985). El niño and variations in climate: large-scale interactions between the ocean and the atmosphere over the tropical pacific can dramatically affect weather patterns around the world. *American Scientist*, *73*(2), 168–177.

Roemmich, D., & Gilson, J. (2009). The 2004–2008 mean and annual cycle of temperature, salinity, and steric height in the global ocean from the argo program.

Progress in oceanography, *82*(2), 81–100.

Schneider, D. P., Deser, C., Fasullo, J., & Trenberth, K. E. (2013). Climate data guide spurs discovery and understanding. *Eos, Transactions American Geophysical Union*, *94*(13), 121–122.

Trenberth, K. E. (1997). The definition of el niño. *Bulletin of the American Meteorological Society*, *78*(12), 2771 - 2778. Retrieved from `https://journals.ametsoc.org/view/journals/bams/78/12/1520-0477_1997_078_2771_tdoeno_2_0_co_2.xml` doi: 10.1175/1520-0477(1997)078⟨2771:TDOENO⟩2.0.CO;2

Wu, S., Fu, F., Wang, L., Yang, M., Dong, S., He, Y., ... Guo, R. (2022). Short-term regional temperature prediction based on deep spatial and temporal networks. *Atmosphere*, *13*(12), 1948.